ARTICLES
https://doi.org/10.1038/s41565-022-01161-w
nature nanotechnology

Check for updates

Nanomedicine platform for targeting activated neutrophils and neutrophil–platelet complexes using an α_1-antitrypsin-derived peptide motif

Michelle A. Cruz[1,15], Dillon Bohinc[2,15], Elizabeth A. Andraska[3,15], Jurgis Alvikas[4], Shruti Raghunathan[5], Nicole A. Masters[6], Nadine D. van Kleef[7], Kara L. Bane[2], Kathryn Hart[5], Kathryn Medrow[5], Michael Sun[5], Haitao Liu[8], Shannon Haldeman[4], Ankush Banerjee[5], Emma M. Lessieur[9], Kara Hageman[5], Agharnan Gandhi[2], Maria de la Fuente[10], Marvin T. Nieman[10], Timothy S. Kern[9,11], Coen Maas[7], Steven de Maat[7], Keith B. Neeves[12], Matthew D. Neal[4], Anirban Sen Gupta[1,5,10,13] ✉ and Evi X. Stavrou[2,13,14] ✉

Targeted drug delivery to disease-associated activated neutrophils can provide novel therapeutic opportunities while avoiding systemic effects on immune functions. We created a nanomedicine platform that uniquely utilizes an α_1-antitrypsin-derived peptide to confer binding specificity to neutrophil elastase on activated neutrophils. Surface decoration with this peptide enabled specific anchorage of nanoparticles to activated neutrophils and platelet–neutrophil aggregates, in vitro and in vivo. Nanoparticle delivery of a model drug, hydroxychloroquine, demonstrated significant reduction of neutrophil activities in vitro and a therapeutic effect on murine venous thrombosis in vivo. This innovative approach of cell-specific and activation-state-specific targeting can be applied to several neutrophil-driven pathologies.

Neutrophils are the first line of host defence, facilitating the containment and destruction of microbial pathogens by releasing granular enzymes, reactive oxygen species and neutrophil extracellular traps (NETs)[1]. While neutrophils are an integral component of the innate immune response, recent evidence supports the unrestricted recruitment and function of activated neutrophils can prolong inflammation and contribute to the development of pathologic conditions such as vascular thrombosis, tumour progression, autoimmune diseases and chronic, non-healing wounds[2]. Therefore, substantial research endeavours have emerged in recent years to develop strategies that modulate neutrophil functions as a treatment for neutrophil-driven pathologies[3–5]. However, studies have revealed considerable challenges with these approaches, primarily stemming from the inhibition of essential neutrophil functions, the limited half-life of therapeutic agents and potential off-target effects associated with systemic delivery[6–8]. Therefore, targeted delivery of therapeutic agents specifically to disease-associated, activated, pro-inflammatory neutrophils can ensure an effective drug half-life, localized action and minimal side effects in treating neutrophil-driven pathologies.

The 'nanomedicine' approach of targeted drug delivery can provide such a strategy, whereby therapeutic agents can be packaged within nanoparticles (NPs), and the particle surface can be decorated with specific ligands that enable selective binding to disease-associated cells and tissues[9–11]. This approach has become highly promising in the targeted delivery of therapeutics in cancer[11,12] and, to some extent, cardiovascular[13] pathologies. Efforts have focused on developing neutrophil-targeted NPs, but the current targeting approaches are not unique or specific to activated neutrophils[14–16]. This presents a remarkable opportunity to develop a neutrophil-specific nanomedicine platform.

Ligand design and NP assembly

To render NP binding specifically to activated neutrophils and platelets, we first identified binding targets on the surface of these cells. For neutrophils, we focused on neutrophil elastase (NE) because (1) it is exposed on the neutrophil surface only upon cell activation and (2) in contrast with other membrane-bound proteins (for example, integrins), NE is exclusively present on neutrophils but not on other leucocyte subsets. Although NE is secreted from neutrophils,

[1]Department of Pathology, Immunology Training Program, CWRU School of Medicine, Cleveland, OH, USA. [2]Department of Medicine, Hematology and Oncology Division, CWRU School of Medicine, Cleveland, OH, USA. [3]Department of Surgery, Division of Vascular Surgery, University of Pittsburgh Medical Center, Pittsburgh, PA, USA. [4]Department of Surgery, Pittsburgh Trauma Research Center, University of Pittsburgh Medical Center, Pittsburgh, PA, USA. [5]Department of Biomedical Engineering, Case Western Reserve University (CWRU), Cleveland, OH, USA. [6]Department of Civil and Environmental Engineering, Colorado School of Mines, Golden, CO, USA. [7]CDL Research, University Medical Center Utrecht, Utrecht University, Utrecht, The Netherlands. [8]Department of Ophthalmology, Children's Hospital of University of Pittsburgh School of Medicine, Pittsburgh, PA, USA. [9]Center for Translational Vision Research, Gavin Herbert Eye Institute, University of California Irvine, Irvine, CA, USA. [10]Department of Pharmacology, CWRU School of Medicine, Cleveland, OH, USA. [11]Veterans Administration Medical Center Research Service, Long Beach, CA, USA. [12]Department of Bioengineering and Pediatrics, Section of Hematology, Oncology, and Bone Marrow Transplant Hemophilia and Thrombosis Center, University of Colorado Denver, Anschutz Medical Campus, Aurora, CO, USA. [13]Case Comprehensive Cancer Center, Case Western Reserve University, Cleveland, OH, USA. [14]Department of Medicine, Section of Hematology-Oncology, Louis Stokes Veterans Administration Medical Center, Cleveland, OH, USA. [15]These authors contributed equally: Michelle A. Cruz, Dillon Bohinc, Elizabeth A. Andraska. ✉e-mail: axs262@case.edu; evi.stavrou@case.edu

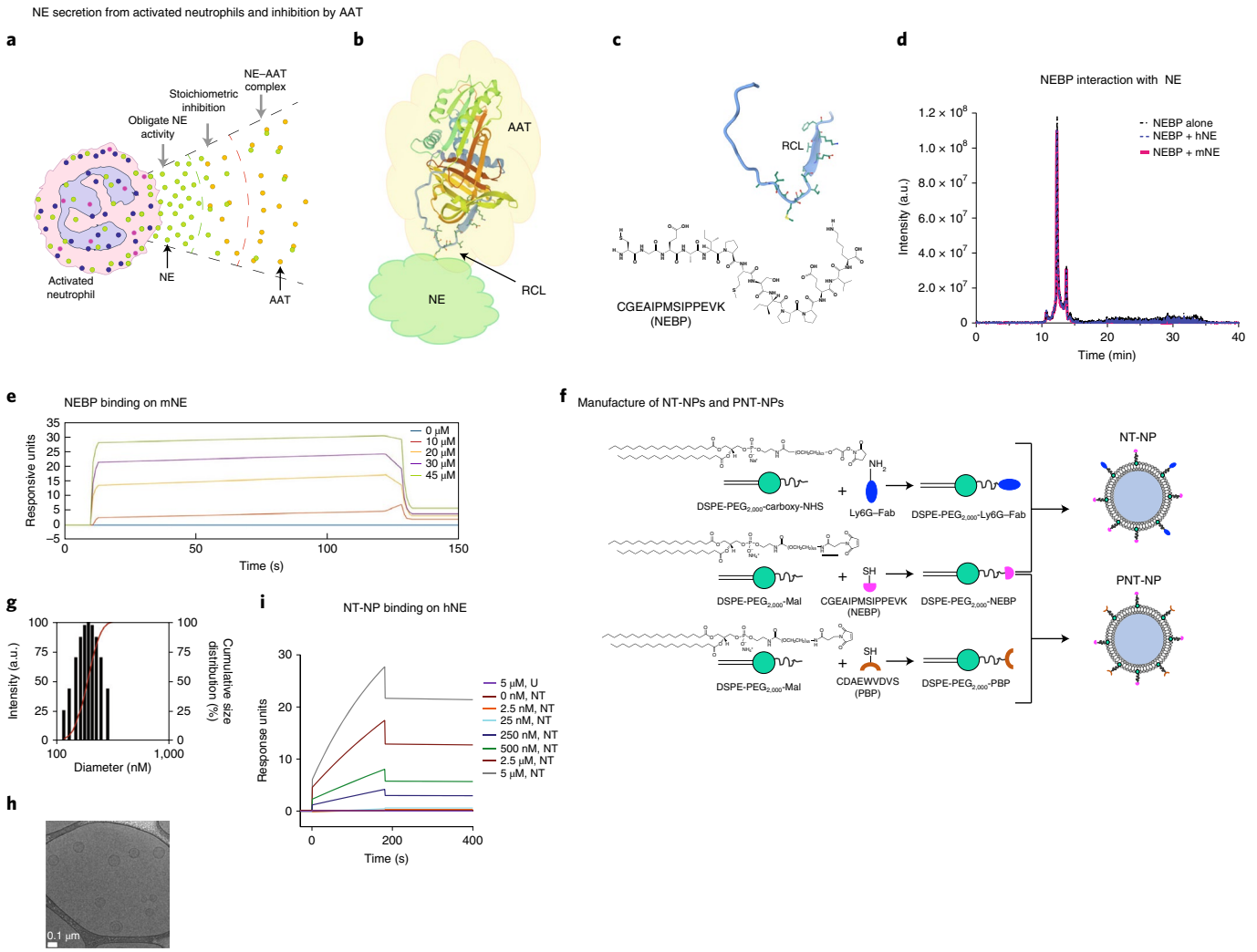

Fig. 1 | Design and characterization of NPs for selective targeting of activated neutrophils. a, Conceptual framework of targeting NE as a strategy to differentiate activated from resting neutrophils. **b**, Physiologically, NE recognizes and binds to a 20 amino acid sequence within the reactive centre loop (RCL; magnified in **c**) of AAT. **c**, A NEBP was designed from the reactive centre loop of AAT. A cysteine at the P7 position was added for subsequent peptide conjugation to NP lipids. Modelling of docking complex with highlighted reactive centre loop and NEBP was performed using native AAT (Protein Data Bank code 1QLP)[20,21]. **d**, Solution-phase hydrolysis of NEBP by NE. High-performance liquid chromatography chromatogram showing pure NEBP (black dashed line) and combination of NEBP with mouse (mNE, red line) or human (hNE, blue dashed line) NE reaction mixture. Data are representative of $n = 3$ individual experiments run in triplicate. **e**, Surface plasmon resonance of NEBP binding to immobilized mNE. Increasing concentrations of NEBP were injected over a mNE-immobilized CM5 chip. **f**, To exclusively target activated neutrophils, Ly6G–Fab (blue) was conjugated to DSPE-PEG-carboxy-NHS; NEBP (purple) was conjugated to DSPE-PEG-Mal. To simultaneously target activated platelets and neutrophils, NEBP and PBP were conjugated to DSPE-PEG-Mal to derive PNT-NPs. DSPE-PEG-NHS, N-hydroxysuccinimide terminated polyethylene glycol conjugated distearyl phosphoethanolamine; Mal, maleimide. **g**, NP size was determined by dynamic light scattering; mean = 200 nm. **h**, Molecular resolution of NPs using cryogenic transmission electron microscopy; $n = 3$ individual experiments. Scale, 0.1 µm. **i**, Kinetic real-time binding of NT-NPs (NT; 0–5 µM) or U-NPs (U; 5 µM) to immobilized hNE; $n = 3$ individual Langmuir binding models run in triplicate.

any free-circulating NE is rapidly and completely neutralized by anti-proteases (Fig. 1a)[17]. However, at the site of secretion, the millimolar concentration of NE outcompetes the micromolar concentration of human α1-antitrypsin[17,18] (AAT; Fig. 1a). For platelet targeting, we focused on P-selectin since this translocates to the plasma membrane only upon platelet activation[19].

To target NE on activated neutrophils, we designed a 14 amino acid peptide (CGEAIPMSIPPEVK) termed NE-binding peptide (NEBP) that binds to NE (Fig. 1b,c)[20,21]. This peptide sequence was derived from the reactive centre loop of AAT, a serpin that physiologically binds to NE (Fig. 1b)[22]. We preserved the methionine at the P1 position and added a cysteine at the P7 position for conjugation of NEBP to lipids for NP construction (Fig. 1f). High-performance liquid chromatography showed no discernible change in the mass spectra of NEBP following incubation with human or murine NE (hNE or mNE; Fig. 1d), supporting that NE does not cleave NEBP. To study the binding of NEBP with mNE, surface plasmon resonance was performed, which showed that NEBP potently bound to mNE with an association rate constant k_{on} of $5.2 \times 10^3\ M^{-1}\ s^{-1}$, a dissociation rate constant k_{off} of $8.31 \times 10^{-6}\ s^{-1}$ and an equilibrium dissociation constant K_D of 1.6 nM (Fig. 1e). Binding between NEBP and free hNE was first characterized with microscale thermophoresis (Supplementary Fig. 1a). Based on microscale thermophoresis measurements, a binding constant of 2.077 ± 1.353 µM was determined for NEBP and hNE, and 0.1375 ± 0.0014 µM for AAT and hNE (Supplementary Fig. 1a). An enzyme-sensitive probe,

N-Methoxysuccinyl-Ala-Ala-Pro-Val-7-amino-4-methylcoumarin, or NMeOSuc-AAPV-AMC (AMC-substrate), was also used to measure the interaction of NEBP with hNE (detection limit for hNE, 0.01 nM). Rising concentrations of AAT (10–120 nM) abolished hNE activity (Supplementary Fig. 1b). NEBP (60–1,000 nM) similarly led to a concentration-dependent decrease in hNE activity (Supplementary Fig. 1b). The second-order rate constant (k_2) of inhibition of NE by AAT was $(7.6 \pm 1.69) \times 10^6\,M^{-1}\,s^{-1}$, whereas for NEBP, k_2 was $(2.5 \pm 1.04) \times 10^5\,M^{-1}\,s^{-1}$ (mean ± s.e.m.). Since hNE is predominantly active on the surface of activated neutrophils[23], we next examined if NEBP can effectively bind to membrane-exposed hNE. We employed a specific small-molecule ratiometric NE reporter based on Forster resonance energy transfer, termed NEmo-2 (detection sensitivity for hNE, 0.02 nM)[23]. *N*-formylmethionine-leucyl-phenylalanine (fMLP) activation of neutrophils led to binding of NEmo-2 to membrane-exposed hNE and resulted in Forster resonance energy transfer reporter cleavage where the donor channel mean fluorescent intensity increased over time, and the acceptor channel mean fluorescent intensity decreased or remained constant (Supplementary Fig. 1c). Incubating activated neutrophils with AAT or NEBP led to a pronounced decrease in Forster resonance energy transfer reporter cleavage compared to fMLP-activated neutrophils (Supplementary Fig. 1c,d). As a control, cultured HEK-293 cells (which do not express NE) were incubated with NEmo-2 and showed no change in donor/acceptor ratio (Supplementary Fig. 1c). Since NEmo reporters provide ~34-fold specificity for hNE over proteinase 3 (PR3; membrane bound) and NEmo-2 does not capture binding to cathepsin G (secreted)[23], we assessed if NEBP interacts with these proteases. Coincubating PR3 or cathepsin G with rising concentrations of NEBP did not lead to a decrease in AMC-substrate fluorescence or succinyl-Ala-Ala-Pro-Phe-*p*-nitroanilide absorbance, respectively (Supplementary Fig. 1e,f), indicating that NEBP does not bind to either protease. Peptide GEAIPMSIPPEVK (termed sNEBP), which lacks the terminal cysteine at the P7 position of NEBP, was similarly found to not interact with PR3 or cathepsin G (Supplementary Fig. 1e,f).

It has been recognized that AAT has the ability to interact with multiple serine protease targets, among them components of the fibrinolytic system[24]. To investigate if NEBP binds to and inhibits non-neutrophil-derived serine proteases like plasmin or tissue plasminogen activator (tPA), we measured plasmin activity, plasmin generation and clot lysis times, with and without NEBP. These studies showed that in contrast to AAT, which abolished all residual plasmin activity, NEBP had no effect when compared to the vehicle (Supplementary Fig. 2a,b). Similarly, NEBP did not affect tPA-induced plasminogen activation (Supplementary Fig. 2c,d) or plasma clot lysis times (Supplementary Fig. 2e–g).

To target P-selectin on activated platelets, we selected the phage-display-generated peptide sequence DAEWVDVS, which has high affinity and specificity to P-selectin ($IC_{50} = 6\,\mu M$) compared to native sialyl Lewis acid ligands[25]. A cysteine was added to this sequence to enable conjugation to lipids for liposomal NP assembly, and this sequence was termed P-selectin binding peptide (PBP; Fig. 1f). We previously demonstrated the utilization of this peptide in NP targeting to ADP-activated platelets[26].

We carried out two combinations of NP surface decoration: (1) we combined two neutrophil-specific ligands, NEBP and an antigen-binding fragment (Fab) derived from anti-Ly6G antibody (clone 1A8)[27], to form heteromultivalent neutrophil-targeted NPs (NT-NPs; Fig. 1f); and (2) we combined NEBP with PBP to create heteromultivalent NPs that simultaneously bind to activated neutrophil–platelet aggregates (henceforth called platelet–neutrophil-targeted NPs, or PNT-NPs; Fig. 1f). Full details on NP assembly[28–30] are provided in the Methods. Mass spectrometry confirmed the successful conjugation of NEBP and PBP peptides and Ly6G–Fab fragment to lipids (Supplementary Fig. 3a–c). NPs were 100–200 nm in diameter, measured by dynamic light scattering and cryo transmission electron microscopy (Fig. 1g,h). Lastly, kinetic surface plasmon resonance experiments showed that assembled NT-NPs bound to NE with a k_{on} of $9.7 \times 10^2\,M^{-1}\,s^{-1}$, k_{off} of 2.94 μM s^{-1} and K_D of 20 nM (Fig. 1i).

NT-NPs selectively bind to activated neutrophils in vitro and in vivo

Ly6G expression, although exclusively found on murine neutrophils, is not specific to activated cells, and high concentrations of Ly6G-specific antibodies can deplete neutrophils[27]. Therefore, we used a considerably higher mole percent of NEBP (2.5 mol%) over Ly6G–Fab (0.1 mol%) for NT-NP decoration (Fig. 2a) and measured the cell viability of murine wild-type neutrophils in the presence of NPs. Neutrophil viability was preserved by >90% when cells were incubated with $3 \times 10^9\,ml^{-1}$ NT-NP (1:100 dilution; Fig. 2b). Based on these results, we utilized $3 \times 10^9\,ml^{-1}$ NPs for all in vitro and in vivo studies with NT-NP.

To assess NP binding specificity towards activated neutrophils in vitro, wild-type neutrophils were incubated with untargeted (U) or targeted (NT) NPs, in the absence or presence of fMLP. Immunofluorescence images showed that U-NPs (rhodamine B (RhB)-labelled only) did not bind to inactive or activated cells (Fig. 2c (upper two panels) and Fig. 2d; $P = 0.14$). By contrast, NT-NPs bound exclusively to activated neutrophils

Fig. 2 | NT-NPs selectively bind to activated neutrophils in vitro and in vivo. a, Schematic representation of targeting ligands on NT-NPs and their binding targets on activated neutrophils. **b**, Neutrophil viability in the presence of rising concentrations of NT-NPs or U-NPs. Mean ± s.e.m., $n = 3$ individual experiments run in triplicate, $^*P = 0.0009$, $^{**}P = 0.0001$, one-way analysis of variance (ANOVA) with Bonferroni correction. NS, not significant. **c**, Confocal microscopy of static murine neutrophils incubated with NT-NPs or U-NPs, in the absence or presence of fMLP. Cells were stained with 4′,6-diamidino-2-phenylindole (DAPI; blue) and NE (green). NPs were labelled with RhB (red). Scale, 10 μm; $n = 3$ independent experiments. **d**, NP binding on neutrophils shown in **c** was quantitated by measuring the residual RhB fluorescence on cells following several washing steps; $n = 3$ independent experiments. Symbols denote high-power fields captured per condition ($n = 16$). Mean ± s.e.m., $^*P < 0.0001$, one-way ANOVA with Bonferroni correction. **e**, Wild-type mice ($n = 3$ per time point) were i.v. administered U-NPs or NT-NPs, and residual NP concentration (conc.) was determined by a RhB fluorescence assay. Mean ± s.e.m., $n = 3$ independent experiments. **f**, Mice were i.v. injected with saline or 1 mg kg^{-1} body weight *Escherichia coli* O111:B4 LPS. Three hours after, anti-Gr-1 antibody (green) mixed with RhB-labelled NPs (U-NPs or NT-NPs) were i.v. injected and allowed to circulate for 40 min before retinas were excised. Retinal vasculature was visualized with Concanavalin A conjugated to fluorescein isothiocyanate. Square and dotted lines in the middle panels demarcate the magnified retinal regions in the right panels. LPS + NT-NP, $n = 6$ mice; LPS + U-NP, $n = 4$ mice; no LPS + NT-NP, $n = 5$ mice; no LPS + U-NP, $n = 6$ mice. Scale, 50 μm. **g**, Representative two-dimensional intensity histograms from retinal images. The *y* axis represents above-zero red pixel intensity (RhB-labelled NPs). The *x* axis indicates above-zero green pixel intensity (adhered neutrophils). **h**, Colocalization analysis of retinal images shown in **f**. Thresholded Manders's correlation coefficient values (tM1 = red overlap with green; tM2 = green overlap with red) are shown among groups. Costes probability value ≥ 95% in LPS + NT-NP; Costes probability value = 0% in all other groups. LPS + NT-NP, $n = 6$ mice; LPS + U-NP, $n = 4$ mice; no LPS + NT-NP, $n = 5$ mice; no LPS + U-NP, $n = 6$ mice. Mean ± s.e.m., $^*P < 0.000001$, $^{**}P = 0.000002$, $^{***}P = 0.000003$, one-way ANOVA with Bonferroni correction.

(lower right panel) but not to inactive cells (Fig. 2c (lower left panel) and Fig. 2d; $P < 0.0001$).

Circulation half-life ($T_{1/2}$), defined as the time where relative residual NP RhB signal is 50%, was determined to be ~8 hours for both U-NPs and NT-NPs (Fig. 2e). To assess the binding specificity of NT-NPs in vivo, systemic inflammation in wild-type mice was induced with intravenous (i.v.) administration of lipopolysaccharide (LPS; 1 mg kg^{-1} body weight), as previously described[31]. Three hours later, mice were injected with RhB-labelled NPs (U-NPs or NT-NPs) and Alexa Fluor-488 anti-Gr-1 antibody. NPs were allowed to circulate for 40 min before mice were perfused with Concanavalin A conjugated to fluorescein isothiocyanate to delineate the retinal microvasculature. Mice injected with phosphate-buffered saline (PBS) and U-NP or NT-NP showed an absence of neutrophil or NP accumulation into retinal capillaries (left upper and left lower panels, Fig. 2f). By contrast, LPS-induced systemic inflammation resulted in robust neutrophil recruitment into the retina (right upper and right lower panels, Fig. 2f). However, NP binding to these activated neutrophils was evident only in mice that had received NT-NPs (right lower panel) and not in mice injected with U-NPs (right upper

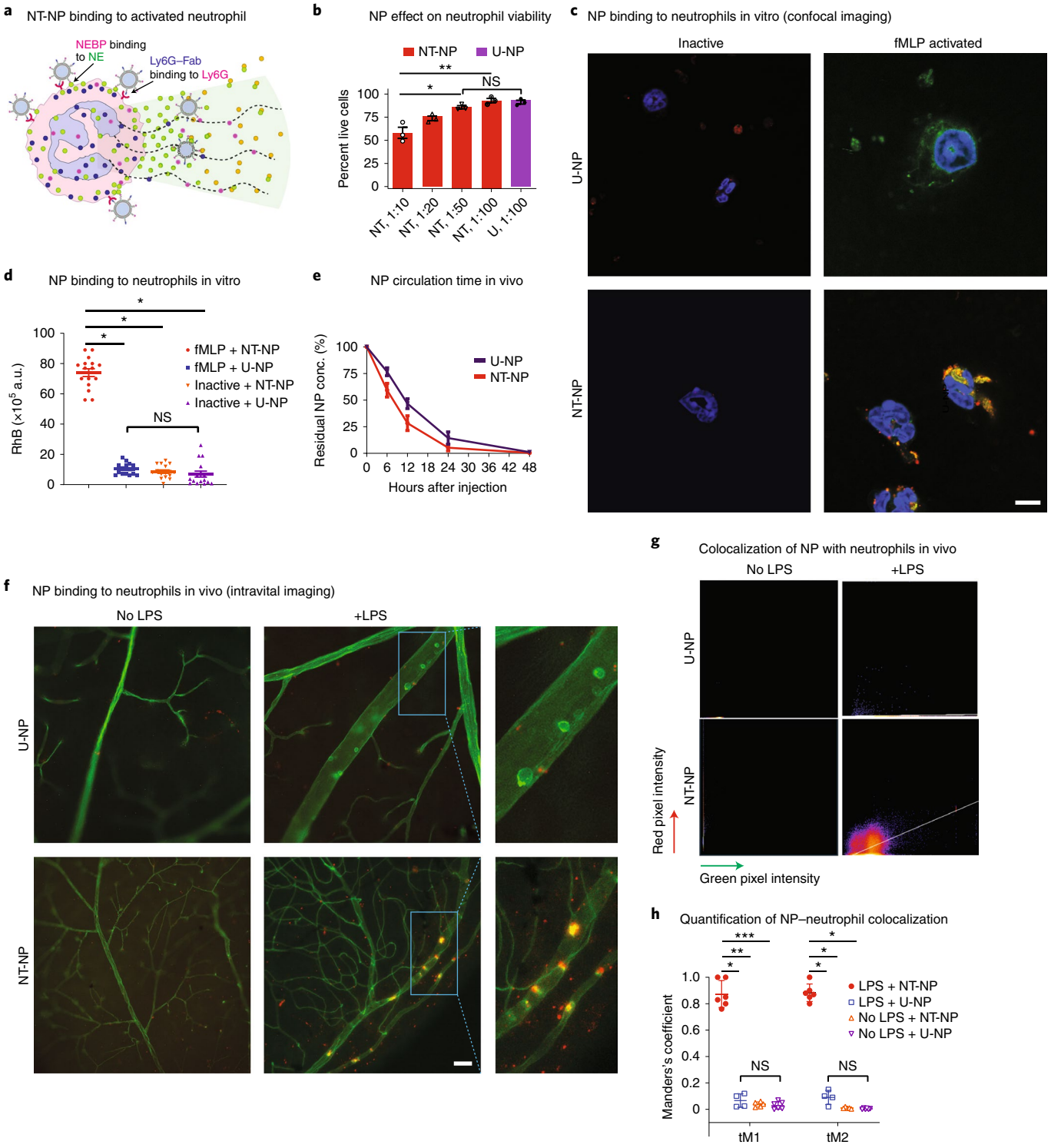

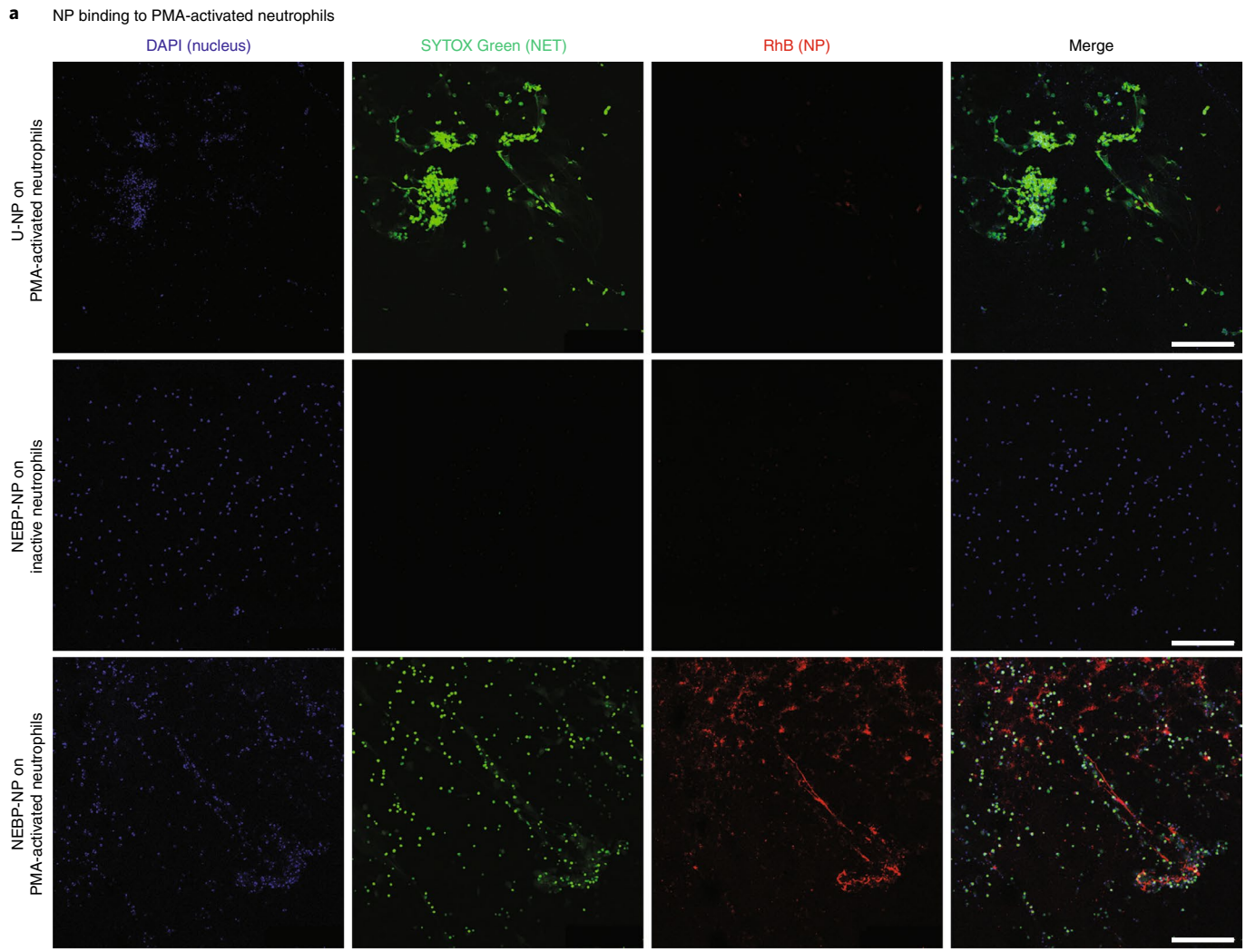

panel, Fig. 2f). Analysis showed minimal colocalization between activated neutrophils and U-NPs but extensive colocalization between activated neutrophils and NT-NPs ($P < 0.000001$; Fig. 2g,h). We next investigated if decorating NPs exclusively with NEBP would maintain binding selectivity and the retention of NPs on activated neutrophils, while allowing studies to be performed with both murine and human cells. These new NPs, termed NEBP-NP, were synthesized as described above. To test NP binding specificity,

Fig. 3 | NT-NPs selectively bind to activated neutrophils and NETs. a, Freshly isolated human neutrophils were treated with media (inactive) or activated with 100 nM PMA in the absence or presence of 3×10^9 ml^{-1} U-NPs or (neutrophil-targeted) NEBP-NPs for 2 h. Cells were subsequently stained with DAPI (blue, nuclei) and SYTOX Green (1 μM, green, extracellular DNA); fixed with 4% formalin for 4 min; and washed in PBS but not permeabilized. NPs are inherently red due to RhB labelling. Fluorescent images were obtained using a Leica TCS SP8 confocal microscope at ×10 magnification. Images are representative of $n=6$ individual experiments. Scale, 250 μm. **b**, Quantitation of NP binding to inactive or PMA-activated neutrophils. Mean ± s.e.m., $n=6$ individual experiments, $^*P=0.001$, $^{**}P=0.0022$, one-way ANOVA with Bonferroni correction. RFU, relative fluorescence units. **c**, Purified human neutrophils were treated with media or neutrophil agonists TNF-α (10 ng ml^{-1}), LPS (5 μg ml^{-1}) and fMLP (1 μM). Cells were coincubated with 3×10^9 ml^{-1} RhB-labelled U-NPs or NEBP-NPs for 1 hour at 37 °C. After several washing and centrifugation steps, cells were fixed and stained with CD66b Alexa Fluor 700 (AF700) and NE Cy5 antibodies. To measure neutrophil–NP binding, cells were first sorted by CD66b positivity, followed by doublet discrimination and gating for hNE. The RhB fluorescence of CD66b and NE double positive single cells was measured. Mean ± s.e.m., $n=3$ individual experiments, $^*P=0.0015$, $^{**}P=0.01$, $^{***}P=0.0046$, one-way ANOVA with Bonferroni correction. MFI, mean fluorescence intensity.

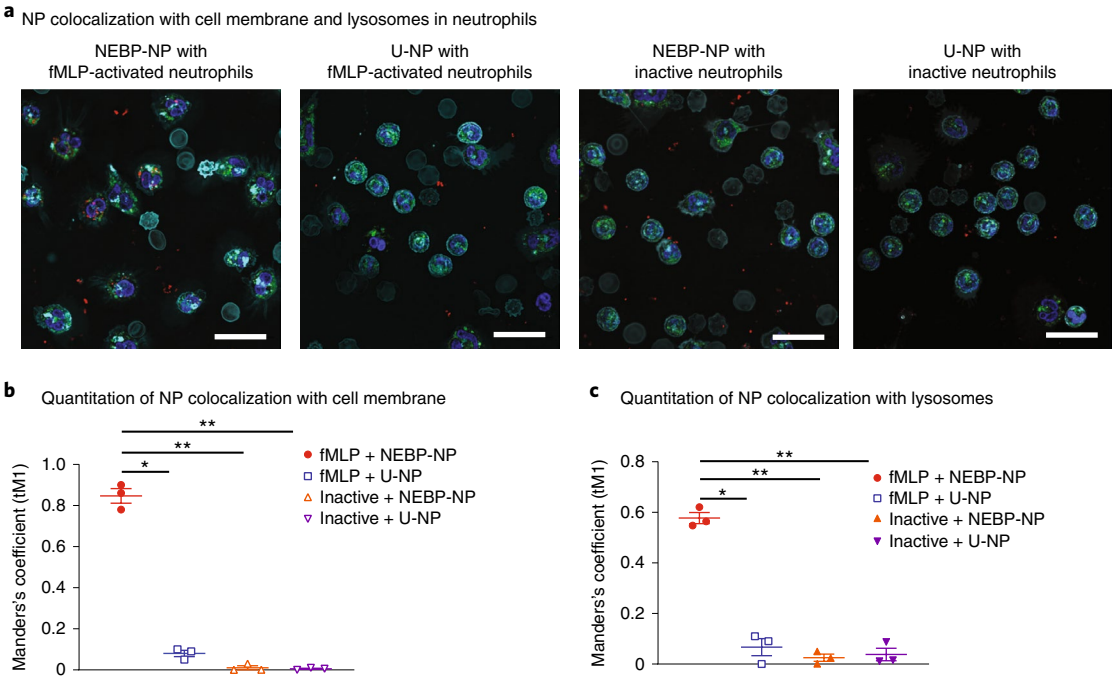

Fig. 4 | Quantitation of NP trafficking by neutrophils. a, Human neutrophils (1×10^6 ml^{-1}) were resuspended in serum-free Dulbecco's modified eagle medium/nutrient mixture F-12 (DMEM/F-12) containing 2 mM $CaCl_2$ and 2 mM $MgCl_2$, plated in 35 mm glass-bottom dishes and allowed to adhere for 15 minutes. Where indicated, cells were activated with 1 μM fMLP in the absence or presence of 3×10^9 ml^{-1} U-NPs or (neutrophil-targeted) NEBP-NPs at 37 °C for 2 h. Cells were maintained alive and were not fixed or permeabilized. On completion of the incubation time, cell components were stained and imaged. Scale, 20 μm; $n=3$ individual experiments. **b**,**c**, For colocalization of NPs with cellular components, thresholded Manders's correlation coefficient values (tM1) are shown among groups for cell membrane–NP interactions (**b**) and lysosome–NP interations (**c**). Costes probability value ≥ 95% in fMLP + NEBP-NP; Costes probability value = 0% in all other groups; $n=3$ individual plates scanned; area, 200 μm × 200 μm. For **b**, mean ± s.e.m., $^*P=0.001$, $^{**}P<0.001$, one-way ANOVA with Bonferroni correction. For **c**, mean ± s.e.m., $^*P=0.018$, $^{**}P=0.00092$, one-way ANOVA with Bonferroni correction.

we performed in vitro immunofluorescence and flow cytometry studies. Human neutrophils were incubated with media or activated with various agonists (phorbol myristate acetate (PMA), tumour necrosis factor alpha (TNF-α), LPS, fMLP), and NEBP-NPs or U-NPs were added. NEBP-NPs bound to activated neutrophils and NETs but did not interact with inactive cells ($P=0.0022$), whereas U-NPs did not colocalize with either inactive or activated neutrophils (Fig. 3a,b). Similarly, flow cytometry showed no significant binding of U-NPs to neutrophils, irrespective of the cell activation state (Fig. 3c). By contrast, the mean fluorescent intensity for RhB was significantly increased when NEBP-NPs were coincubated with activated neutrophils (Supplementary Fig. 4a) but not with inactive cells (Fig. 3c).

Investigations next examined how neutrophils process NEBP-NPs. Live human neutrophils were treated with media or stimulated with 1 μM fMLP and coincubated with U-NPs or NEBP-NPs for 2 hours. On completion of incubation, the plasma membrane, lysosomes and nuclei were fluorescently labelled and analysed with confocal imaging. U-NPs did not localize on the surface of inactive neutrophils, as seen by the lack of colocalization between RhB and plasma membrane stains (Supplementary Fig. 5 and Fig. 4a–c). Similarly, when U-NPs were incubated with fMLP-activated neutrophils, no NP retention or cell uptake was observed. NEBP-NPs coincubated with inactive neutrophils did exhibit minimal NP binding on the plasma membrane, likely due to a degree of neutrophil activation after 2 hours of incubation (Supplementary Fig. 5 and Fig. 4a–c). NEBP-NPs incubated with fMLP-activated cells significantly bound to the neutrophil surface and, in contrast to any other condition, NEBP-NPs were also internalized (Supplementary Fig. 5 and Fig. 4a–c). Composite images revealed partial intracellular trafficking of NEBP-NPs to lysosomes, albeit the largest NP proportion remained bound at the plasma membrane (Supplementary Fig. 5 and Fig. 4a–c).

PNT-NPs effectively target activated platelet–neutrophil aggregates

In recent years, multiple animal and clinical studies have identified that inflammatory processes and deep vein thrombosis (DVT) are intricately linked[32–34]. Therefore, we hypothesized that PNT-NPs can be utilized to target activated platelet–neutrophil complexes (Fig. 5a). Human platelets and neutrophils, activated with 20 nM thrombin and 1 μM fMLP, respectively, were incubated with 3×10^9 ml^{-1} RhB-labelled NPs (U-NP, NEBP-NP, PBP-NP or PNT-NP) and images were used to quantitate RhB, a measure of NP retention on cell aggregates (Fig. 5b). There was minimal RhB fluorescence when U-NPs were incubated with activated platelets and neutrophils (Fig. 5b (middle row panels) and Fig. 5c). By contrast, PNT-NPs were able to significantly bind to activated platelets and neutrophils (Fig. 5b (bottom row panels) and Fig. 5c) compared to U-NPs ($P<0.001$). Single decoration of NPs with NEBP or PBP each resulted in significantly higher NP targeting to activated platelets and neutrophils compared to U-NP ($P<0.0001$), but combinatorial decoration with NEBP and PBP synergistically conferred significantly higher binding efficacy of PNT-NPs compared to either NEBP-NPs or PBP-NPs ($P<0.0001$; Supplementary Fig. 6a,b). In flow cytometry analyses, no significant increase in RhB median fluorescent intensity occurred when inactive neutrophils (IN) and platelets (IP) were coincubated with U-NPs or PNT-NPs (Fig. 5d (upper two panels) and Fig. 5e). By contrast, coincubation of activated cell complexes with PNT-NP (Fig. 5d, lower two panels) resulted in a significant increase in RhB median fluorescent intensity compared to treatment with U-NPs (Fig. 5d,e).

The above results provided the rationale to study whether PNT-NPs can bind to a DVT-relevant thrombotic niche under flow for potential drug delivery. For this, we employed a custom DVT microfluidic model where clot formation is initiated by immobilized tissue factor and supported by the low shear vortical flows within the valve pocket (Fig. 6a)[35]. Time-lapse video microscopy demonstrated significantly increased accumulation of PNT-NPs compared to U-NPs in the thrombus forming within the valve pocket (Fig. 6b). PNT-NP binding to recruited platelets and neutrophils was observed at early time points, and for several time frames, PNT-NPs could be seen 'following' an activated neutrophil or platelet (Supplementary Video 1). By contrast, U-NPs did not adhere at the thrombus site until NET and fibrin formation had occurred (Fig. 6b), indicating that NPs were non-specifically trapped within the thrombotic niche rather than specifically binding to the thrombus (Supplementary Fig. 7a,b and Supplementary Video 2). Soluble P-selectin did not interfere with NP binding to activated platelets[36] (Supplementary Fig. 8a,b).

Targeted therapeutic effect of PNT-NP nanomedicine in vivo

For proof-of-concept DVT studies with drug-loaded NPs, we chose to use hydroxychloroquine (HCQ) since (1) we previously showed that intraperitoneal administration of HCQ reduced thrombus burden in murine models of trauma[37]; (2) HCQ is an autophagy inhibitor and can potentially impact neutrophil functions[38]; and (3) there is considerable dose-limiting toxicity with systemic HCQ treatment[39–41]. HCQ was encapsulated within PNT-NPs to yield HCQ_PNT-NPs (Supplementary Fig. 9a,b). When neutrophils were incubated with free HCQ, cell viability fell below 90% at HCQ concentrations equal to or higher than 2×10^3 ng ml^{-1} (Fig. 6c). By contrast, neutrophil incubation with HCQ_PNT-NPs did not result in cell cytotoxicity across all tested concentrations (0–3×10^6 ng ml^{-1}; Fig. 6c). We next investigated if HCQ influences key neutrophil effectors involved in sterile inflammatory and thrombotic processes, among them NE secretion and NET-osis[42]. To allow comparisons between free HCQ and HCQ-loaded PNT-NPs while not affecting neutrophil viability, all in vitro mechanistic studies were performed at a fixed HCQ concentration (350 ng ml^{-1}), which fell well within the range of non-cytotoxic dosing (Fig. 6c). Treatment of fMLP-stimulated neutrophils with unencapsulated HCQ led to a significant reduction in NE activity compared to fMLP without HCQ ($P<0.0001$). Importantly, treatment of neutrophils with the same concentration of HCQ packaged in PNT-NPs (HCQ_PNT-NPs) resulted in a comparable reduction of NE activity as with free HCQ ($P<0.0001$ versus fMLP; Fig. 6d). Since NE associates with NETs[32], we studied whether a HCQ-mediated decrease in extracellular NE activity can translate into reduced NET formation. fMLP stimulation led to a rapid increase in citrullinated histone H3 expression, which was significantly reduced by free HCQ ($P<0.0001$; Supplementary Fig. 4c,d and Fig. 6e). Notably, HCQ_PNT-NPs resulted in the highest reduction in citrullinated histone H3 expression ($P<0.0001$ versus fMLP; Fig. 6e). For in vivo studies, we established that the circulation half-life of PNT-NPs was similar to that of NT-NPs at ~8 hours (Supplementary Fig. 10a). In terms of systemic safety, i.v.-free HCQ was found to be highly lethal to mice, whereas i.v. HCQ_PNT-NPs had no effect on survival (final HCQ, 350 μg per mouse in both groups; Fig. 6f). For therapeutic studies, we utilized a murine model of DVT in which flow restriction induces thrombosis in the inferior vena cava (IVC; Fig. 6g)[32]. Saline (no treatment), empty untargeted NPs (U-NPs), HCQ_U-NPs (containing HCQ but no surface decorations) or HCQ_PNT-NPs (codecorated with NEBP + PBP and loaded with HCQ) were i.v. administered 30 minutes prior to surgical induction of IVC ligation, and IVC thrombi were harvested 24 hours later. Lack of NP surface decorations (U-NP) resulted in thrombus weights identical to control wild-type mice, irrespective of HCQ loading (Fig. 6h). Distinctly, PNT-NPs loaded with HCQ led to significantly smaller thrombi compared to every other group (Fig. 6h). Systemic i.v. administered HCQ at a 350 μg dose did not result in significantly lower thrombus weights compared to no treatment ($P=0.1$; Supplementary Fig. 10b), likely due to the low number of surviving animals.

To establish the selective contribution of neutrophil targeting and platelet targeting to the therapeutic effect of thrombus weight reduction, HCQ was encapsulated in NPs bearing NEBP (HCQ_NEBP-NPs) or PBP (HCQ_PBP-NPs) decorations only.

Fig. 5 | Heteromultivalent NPs selectively bind to activated platelet–neutrophil complexes in vitro. a, Schematic illustration of PNT-NPs. The combined decoration of NPs with a PBP (targeting P-selectin) and NEBP (targeting NE) enables PNT-NPs to bind simultaneously and selectively to activated platelet–neutrophil complexes. **b**, Freshly isolated human neutrophils and platelets were activated with 1 μM fMLP and 20 nM thrombin prior to being coincubated with RhB-labelled (red) U-NPs or PNT-NPs. Platelets were stained with calcein (green), and nuclei corresponding to activated neutrophils were counterstained with DAPI (blue). Representative images show that PNT-NPs (third row panels) bound to activated platelet–neutrophil aggregates, but undecorated U-NPs (second row panels) did not. Images are representative of $n=10$–11 individual experiments run in triplicate. Scale, 100 μm. **c**, NP retention on activated platelet–neutrophil complexes was measured by quantitating residual RhB fluorescence. U-NP, $n=10$ individual samples; PNT-NP, $n=11$ individual samples; all run in triplicate. Mean ± s.e.m., $^{**}P<0.01$ by Student's t-test. **d**, Human neutrophils were either left untreated or activated with fMLP and incubated with U-NPs or PNT-NPs. Representative flow cytograms (left upper and left lower panels) of NP retention on inactive (IN) or activated (AN) neutrophils; $n=5$–6 individual experiments run in triplicate. Human platelets were left untreated or activated with 20 nM thrombin, in the absence or presence of U-NPs or PNT-NPs. Representative flow cytograms (right upper and right lower panels) of $n=5$–6 individual experiments run in triplicate. AP, activated platelets. **e**, Cell–NP binding to IN, AN, IP or AP was quantitated by measuring RhB fluorescence intensity; $n=5$–6 individual experiments run in triplicate. Data are presented as mean ± s.e.m., $^{**}P<0.0017$, $^{***}P=0.0008$, $^{****}P<0.0001$, ordinary two-way ANOVA.

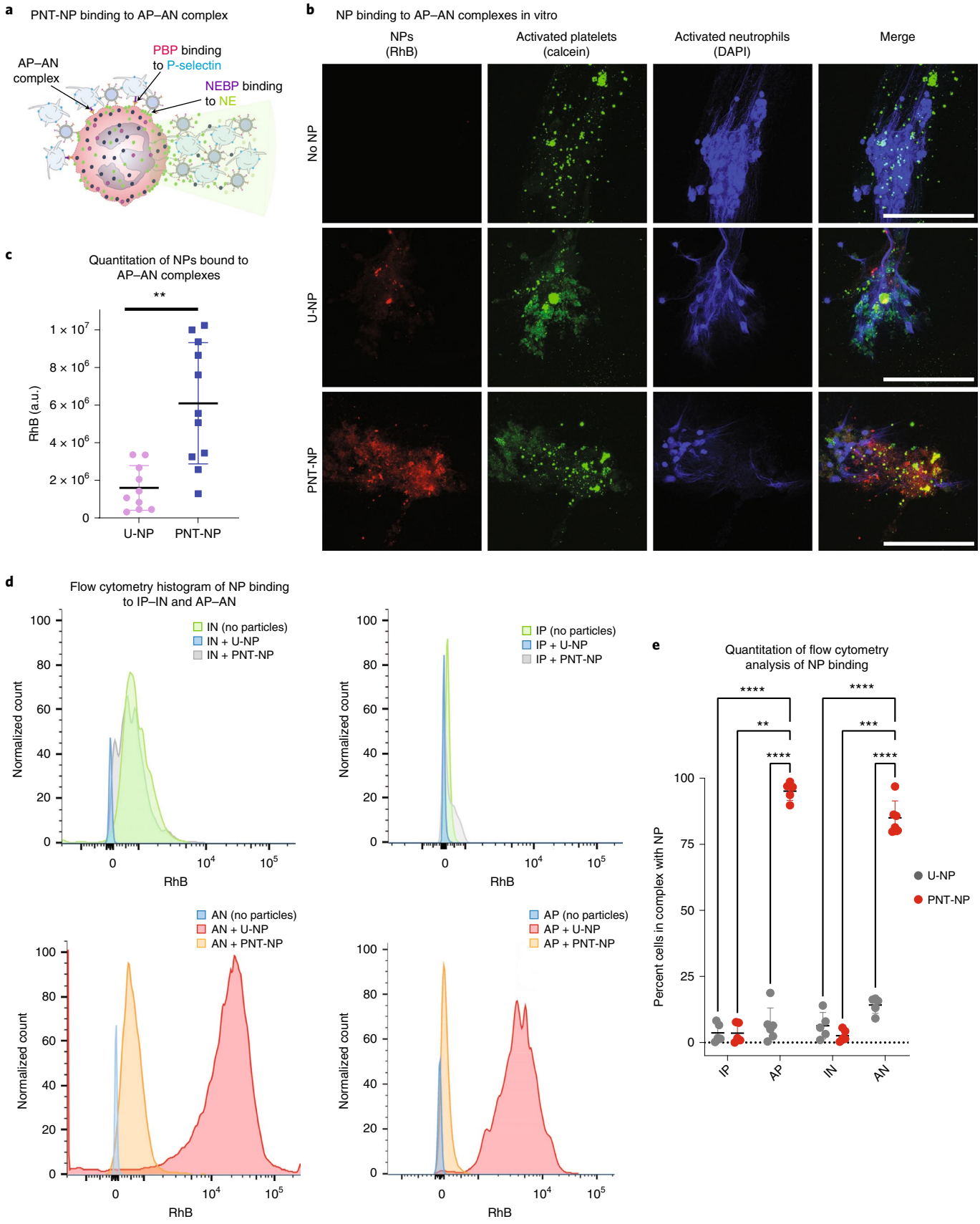
a
PNT-NP binding to AP–AN complex
AP–AN complex
PBP binding to P-selectin
NEBP binding to NE
b
NP binding to AP–AN complexes in vitro
NPs (RhB)
Activated platelets (calcein)
Activated neutrophils (DAPI)
Merge
No NP
U-NP
PNT-NP
c
Quantitation of NPs bound to AP–AN complexes
**
RhB (a.u.)
1 × 10^7
8 × 10^6
6 × 10^6
4 × 10^6
2 × 10^6
0
U-NP
PNT-NP
d
Flow cytometry histogram of NP binding to IP–IN and AP–AN
IN (no particles)
IN + U-NP
IN + PNT-NP
IP (no particles)
IP + U-NP
IP + PNT-NP
AN (no particles)
AN + U-NP
AN + PNT-NP
AP (no particles)
AP + U-NP
AP + PNT-NP
Normalized count
RhB
e
Quantitation of flow cytometry analysis of NP binding
Percent cells in complex with NP
U-NP
PNT-NP
IP
AP
IN
AN

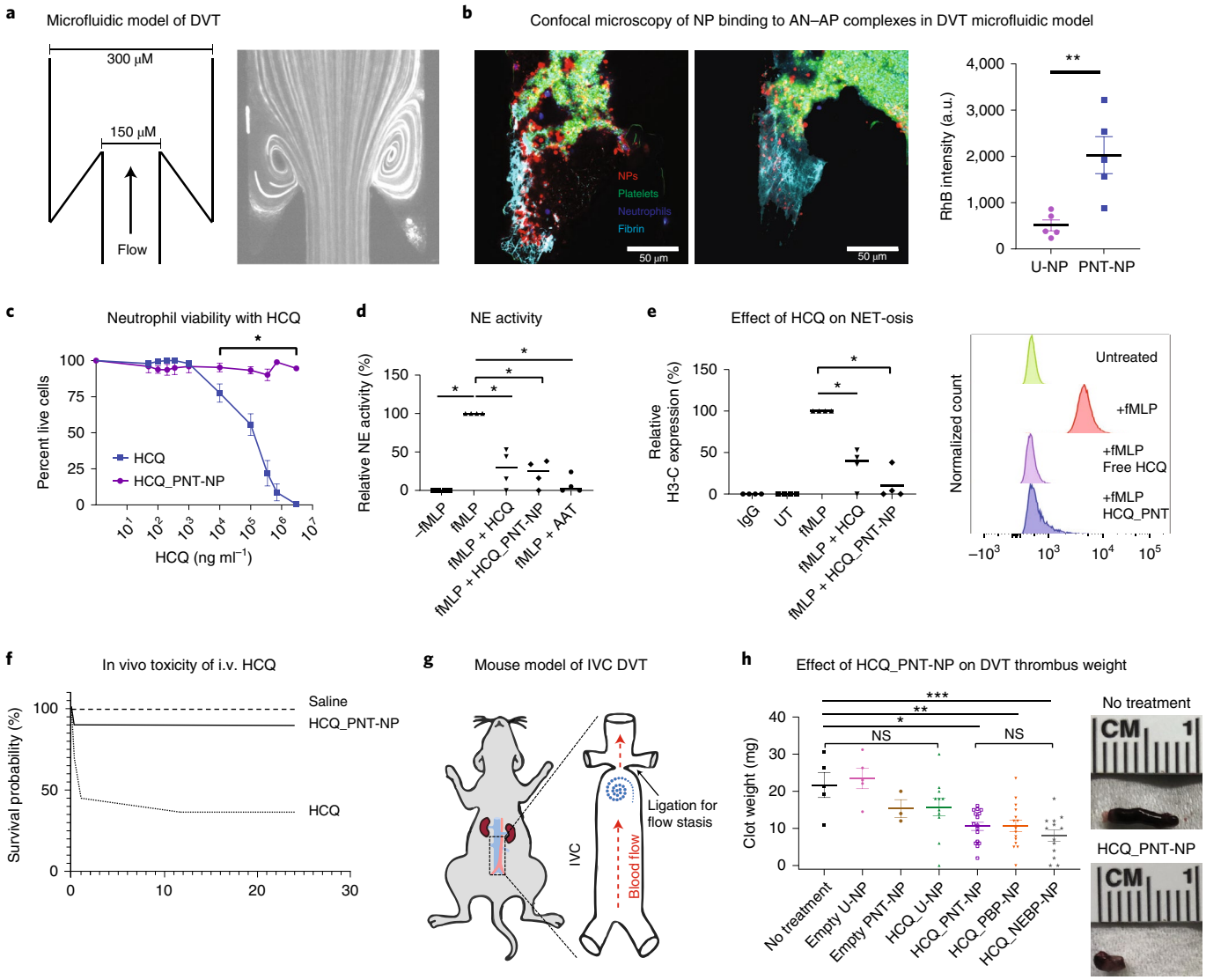

Fig. 6 | PNT-NPs bind to thromboinflammatory sites and effectively deliver therapeutic cargo to reduce thrombus size. a, Schematic of microfluidic set-up. Image of 1 μm polystyrene particle streak lines demonstrating vorticle flows recirculating in valve pockets. **b**, Maximum projections of confocal stack after 30 min of blood flow. NPs are in red, human platelets in green, neutrophils in blue and fibrin(ogen) in cyan. RhB fluorescent intensity within microchannels is shown at the right. Mean ± s.e.m., $n = 3$ individual experiments run in triplicate, $^{*}P = 0.006$, two-sided Student's t-test. **c**, Neutrophil viability in the presence of free HCQ or HCQ_PNT-NPs. Mean ± s.e.m., $n = 3$ individual experiments run in triplicate, $^{*}P = 0.0079$ compared to initial (100%) viability, ordinary two-way ANOVA. **d**, NE activity of human neutrophils pretreated with AAT, free HCQ or HCQ_PNT-NPs for 2 h prior to stimulation with fMLP. Mean ± s.e.m., $n = 3$ individual experiments run in triplicate, $^{**}P < 0.0001$, one-way ANOVA with Bonferroni correction. **e**, Flow cytometry analysis of NET formation in human neutrophils pretreated with free HCQ or HCQ_PNT-NP prior to stimulation with fMLP. UT denotes untreated neutrophils. Data are presented as relative expression of citrullinated histone H3 (H3-C). Mean ± s.e.m., $n = 4$ experiments, $^{*}P < 0.0001$, one-way ANOVA with Bonferroni correction. **f**, Kaplan–Meier survival analysis in mice i.v treated with saline (control), free HCQ or HCQ_PNT-NPs. **g**, Schematic representation of deep venous thrombosis model. **h**, Prior to IVC ligation, mice were i.v. injected with saline (no treatment, $n = 5$); empty U-NPs ($n = 5$); empty PNT-NPs ($n = 3$); HCQ_U-NPs ($n = 10$); HCQ_PNT-NPs ($n = 16$); HCQ_NEBP-NPs ($n = 13$); or HCQ_PBP-NPs ($n = 13$). Thrombi were harvested at 24 h. Each symbol represents an individual mouse. Mean ± s.e.m., $^{*}P = 0.0065$, $^{**}P = 0.01$, $^{***}P = 0.004$, one-way ANOVA with Bonferroni correction. Gross images of harvested thrombi from control (top panel) and mice i.v. treated with HCQ_PNT-NPs (bottom panel).

Additionally, DVT studies were performed using drug-loaded NEBP-NPs at full (3×10^9 ml^{-1}), half (1.5×10^9 ml^{-1}) and double (6×10^9 ml^{-1}) the dose. By comparison, i.v.-free HCQ was used at half the full dose (175 μg per mouse). Treatment with HCQ-loaded NEBP-NPs at half the dose (1/2 × HCQ_NEBP-NPs) led to a significant reduction in thrombus weights compared to no treatment and to free 1/2 × HCQ (Supplementary Fig. 10b). Doubling the dose of HCQ_NEBP-NPs to 6×10^9 ml^{-1} (2 × HCQ_NEBP-NPs) was well tolerated in mice without an increase in mortality and significantly reduced thrombus weights ($P = 0.03$) but added no benefit to thrombus weight reduction when compared to lower doses of HCQ_NEBP-NPs. When comparing PNT-NPs versus PBP-NPs versus NEBP-NPs, we found no significant differences in therapeutic efficacy (Fig. 6h), suggesting that in a milieu where activated neutrophils and platelets are similarly represented, targeting either cell population can be highly efficacious and safer than systemic drug treatment (compare 1/2 × HCQ alone versus 1/2 × HCQ_NEBP-NPs; $P = 0.0065$).

On completion of the DVT studies, we retrieved various clearance organs to assess the NP biodistribution. The RhB signal at 24 hours was significantly low, indicating that a very small percentage dose either cleared or remained in these organ beds (Supplementary Fig. 10c).

Conclusions

Increasing evidence has uncovered significant phenotypic heterogeneity within the neutrophil population. Functional characterization of neutrophils isolated from individuals with autoimmune diseases, chronic infections and cancer identified a distinct subpopulation that exhibits a pro-inflammatory, activated phenotype with prolonged lifespan and susceptibility to form NETs[43]. In this context, we aimed to develop a therapeutic strategy that specifically targets these pathogenic neutrophil subsets without the ubiquitous inhibition of resting cells.

In designing an activation-state-specific NP, we chose to target NE since several pathogenic, pro-inflammatory functions of neutrophils (for example, tissue proteolysis and NET-osis) are in part elastase dependent. Studies with human proteins confirmed that NEBP avidly binds to hNE but not to PR3, cathepsin G or non-neutrophil proteases. Prior studies have shown that several factors influence serpin behaviour, among them (1) the length of the reactive centre loop, (2) secondary binding sites outside of the reactive centre loop and (3) intramolecular control of the reactive centre loop conformation[44]. The above suggest that the binding kinetics and activity of intact AAT may not be identical to that of reactive-centre-loop-derived peptides such as NEBP.

To our knowledge, this is the first demonstration of specific targeting of activated neutrophils. Other nanomedicine systems have reported neutrophil-specific targeting; however, their design reveals the potential for cross-reactivity with other immune cells. For example, targeting crystallizable fragment (Fc)-gamma receptors[14,15] would also affect B lymphocytes, natural killer cells and macrophages, whereas targeting of scavenger receptors would affect all myeloid cells, as well as dendritic and endothelial cells[45]. Although NE may not be the pathophysiologic driver in all neutrophil-mediated diseases, its cell-specific expression, distinct surface retention on activated neutrophils and presence on NETs has been widely demonstrated. These properties confer NE with a unique ability to serve as 'bait', capturing targeted NPs for localized drug delivery. Considering an average neutrophil lifespan of ~18.5 h (ref. [46]), the NP half-life at steady state would be comparable for meaningful targeting of pathogenic cells. Although in vivo use of liposomal NPs has proven safe[47], further work is required to better determine the pharmacokinetics, elimination and safety profile of NEBP-NPs and PNT-NPs. Trafficking studies showed that intracellular movement of NEBP-NPs was detectable only in the activated group of neutrophils, suggesting that the rate-limiting step for NP internalization is the binding of NEBP to hNE. This would resemble a process of 'receptor-mediated endocytosis', which has been described for hNE interactions with yeast[48].

Finally, we demonstrate therapeutic proof-of-concept studies of drug-loaded PNT-NPs[49]. We provide additional mechanistic insight that HCQ effectively downregulates neutrophil degranulation and NET formation. While HCQ is currently approved in an oral formulation, its systemic use has been linked to several adverse events[39–41]. The present findings should form the basis for future studies to test therapeutic agents that have a limited half-life, a narrow therapeutic window or decreased tissue penetration. Our group has previously shown that the axis of Factor XII and urokinase plasminogen activator receptor upregulates neutrophil functions to lead to enhanced cell migration and NET-osis[50]. Abrogating Factor XII-mediated effects, specifically in neutrophils, improved cutaneous wound healing and restricted ovarian tumour growth and dissemination[50,51]. In non-sterile inflammation, exuberant activation of neutrophils was linked to microvascular thrombosis and tissue injury in severe acute respiratory syndrome coronavirus 2 infection[52]. Therefore, neutrophil-targeted strategies, tailored to treat activated cells and resolve perpetuating inflammation, can potentially be a safe and highly efficient approach to neutralize the harmful pathologic effects driven by neutrophils, promote healing and preserve innate immunity or haemostasis.

Online content

Any methods, additional references, Nature Research reporting summaries, source data, extended data, supplementary information, acknowledgements, peer review information; details of author contributions and competing interests; and statements of data and code availability are available at https://doi.org/10.1038/s41565-022-01161-w.

Received: 21 February 2021; Accepted: 24 May 2022;
Published online: 18 July 2022

References

1. Brinkmann, V. et al. Neutrophil extracellular traps kill bacteria. *Science* **303**, 1532–1535 (2004).
2. Sorvillo, N. et al. Extracellular DNA NET-works with dire consequences for health. *Circ. Res.* **125**, 470–488 (2019).
3. Albadawi, H. et al. Effect of DNase I treatment and neutrophil depletion on acute limb ischemia-reperfusion injury in mice. *J. Vasc. Surg.* **64**, 484–493 (2016).
4. Ramacciotti, E. et al. P-selectin/PSGL-1 inhibitors versus enoxaparin in the resolution of venous thrombosis: a meta-analysis. *Thromb. Res.* **125**, e138–e142 (2010).
5. Kim, K. et al. NOX2 is critical for heterotypic neutrophil-platelet interactions during vascular inflammation. *Blood* **126**, 1952–1964 (2015).
6. Li, P. et al. PAD4 is essential for antibacterial innate immunity mediated by neutrophil extracellular traps. *J. Exp. Med.* **207**, 1853–1862 (2010).
7. Cho, H. et al. Insulin resistance and a diabetes mellitus-like syndrome in mice lacking the protein kinase Akt2 (PKB beta). *Science* **292**, 1728–1731 (2001).
8. Ridker, P. M. et al. Antiinflammatory therapy with canakinumab for atherosclerotic disease. *N. Engl. J. Med.* **377**, 1119–1131 (2017).
9. Xu, L. et al. Heterobivalent ligands target cell-surface receptor combinations in vivo. *Proc. Natl Acad. Sci. USA* **109**, 21295–21300 (2012).
10. Gunawan, R. C., Almeda, D. & Auguste, D. T. Complementary targeting of liposomes to IL-1α and TNF-α activated endothelial cells via the transient expression of VCAM1 and E-selectin. *Biomaterials* **32**, 9848–9853 (2011).
11. Sapra, P. & Allen, T. M. Improved outcome when B-cell lymphoma is treated with combinations of immunoliposomal anticancer drugs targeted to both the CD19 and CD20 epitopes. *Clin. Cancer Res.* **10**, 2530–2537 (2004).
12. Kanapathipillai, M., Brock, A. & Ingber, D. E. Nanoparticle targeting of anti-cancer drugs that alter intracellular signaling or influence the tumor microenvironment. *Adv. Drug Deliv. Rev.* **79**, 107–118 (2014).
13. Anselmo, A. C. et al. Platelet-like nanoparticles: mimicking shape, flexibility, and surface biology of platelets to target vascular injuries. *ACS Nano* **8**, 11243–11253 (2014).
14. Wang, Z. et al. Prevention of vascular inflammation by nanoparticle targeting of adherent neutrophils. *Nat. Nanotechnol.* **9**, 204–210 (2014).
15. Chu, D. et al. Nanoparticle targeting of neutrophils for improved cancer immunotherapy. *Adv. Healthc. Mater.* **5**, 1088–1093 (2016).
16. Robertson, J. D. et al. Targeting neutrophilic inflammation using polymersome-mediated cellular delivery. *J. Immunol.* **198**, 3596–3604 (2017).
17. Liou, T. G. & Campbell, E. J. Nonisotropic enzyme–inhibitor interactions: a novel nonoxidative mechanism for quantum proteolysis by human neutrophils. *Biochemistry* **34**, 16171–16177 (1995).
18. Owen, C. A. et al. Cell surface-bound elastase and cathepsin G on human neutrophils: a novel, non-oxidative mechanism by which neutrophils focus and preserve catalytic activity of serine proteinases. *J. Cell Biol.* **131**, 775–789 (1995).
19. Stenberg, P. E. et al. A platelet alpha-granule membrane protein (GMP-140) is expressed on the plasma membrane after activation. *J. Cell Biol.* **101**, 880–886 (1985).
20. Elliott, P. R. et al. Inhibitory conformation of the reactive loop of α_1-antitrypsin. *Nat. Struct. Biol.* **3**, 676–681 (1996).
21. Elliott, P. R. et al. Topography of a 2.0 Å structure of α_1-antitrypsin reveals targets for rational drug design to prevent conformational disease. *Protein Sci.* **9**, 1274–1281 (2000).
22. Forsyth, S., Horvath, A. & Coughlin, P. A review and comparison of the murine α_1-antitrypsin and α_1-antichymotrypsin multigene clusters with the human clade A serpins. *Genomics* **81**, 336–345 (2003).

23. Gehrig, S., Mall, M. A. & Schultz, C. Spatially resolved monitoring of neutrophil elastase activity with ratiometric fluorescent reporters. *Angew. Chem. Int. Ed.* **51**, 6258–6261 (2012).
24. Beatty, K., Bieth, J. & Travis, J. Kinetics of association of serine proteinases with native and oxidized α-1-proteinase inhibitor and α-1-antichymotrypsin. *J. Biol. Chem.* **255**, 3931–3934 (1980).
25. Appeldoorn, C. C. et al. Rational optimization of a short human P-selectin-binding peptide leads to nanomolar affinity antagonists. *J. Biol. Chem.* **278**, 10201–10207 (2003).
26. Modery, C. L. et al. Heteromultivalent liposomal nanoconstructs for enhanced targeting and shear-stable binding to active platelets for site-selective vascular drug delivery. *Biomaterials* **32**, 9504–9514 (2011).
27. Daley, J. M. et al. Use of Ly6G-specific monoclonal antibody to deplete neutrophils in mice. *J. Leukoc. Biol.* **83**, 64–70 (2008).
28. Elliott, J. T. & Prestwich, G. D. Maleimide-functionalized lipids that anchor polypeptides to lipid bilayers and membranes. *Bioconjug. Chem.* **11**, 832–841 (2000).
29. Zhang, H. Thin-film hydration followed by extrusion method for liposome preparation. *Methods Mol. Biol.* **1522**, 17–22 (2017).
30. Hope, M. J. et al. Reduction of liposome size and preparation of unilamellar vesicles by extrusion techniques. *Liposome Technol.* **1**, 123–139 (1993).
31. Bennewitz, M. F. et al. Lung vaso-occlusion in sickle cell disease mediated by arteriolar neutrophil-platelet microemboli. *JCI Insight* **2**, e89761 (2017).
32. von Bruhl, M. L. et al. Monocytes, neutrophils, and platelets cooperate to initiate and propagate venous thrombosis in mice in vivo. *J. Exp. Med.* **209**, 819–835 (2012).
33. Martinod, K. et al. Neutrophil histone modification by peptidylarginine deiminase 4 is critical for deep vein thrombosis in mice. *Proc. Natl Acad. Sci. USA* **110**, 8674–8679 (2013).
34. Middleton, E. A. et al. Neutrophil extracellular traps contribute to immunothrombosis in COVID-19 acute respiratory distress syndrome. *Blood* **136**, 1169–1179 (2020).
35. Lehmann, M. et al. Platelets drive thrombus propagation in a hematocrit and glycoprotein VI–dependent manner in an in vitro venous thrombosis model. *Arterioscler. Thromb. Vasc. Biol.* **38**, 1052–1062 (2018).
36. Ramacciotti, E. et al. Evaluation of soluble P-selectin as a marker for the diagnosis of deep venous thrombosis. *Clin. Appl. Thromb. Hemost.* **17**, 425–431 (2011).
37. Dyer, M. R. et al. Platelet-derived extracellular vesicles released after trauma promote hemostasis and contribute to DVT in mice. *J. Thromb. Haemost.* **17**, 1733–1745 (2019).
38. Bhattacharya, A. et al. Autophagy is required for neutrophil-mediated inflammation. *Cell Rep.* **12**, 1731–1739 (2015).
39. Melles, R. B. & Marmor, M. F. The risk of toxic retinopathy in patients on long-term hydroxychloroquine therapy. *JAMA Ophthalmol.* **132**, 1453–1460 (2014).
40. Mercuro, N. J. et al. Risk of QT interval prolongation associated with use of hydroxychloroquine with or without concomitant azithromycin among hospitalized patients testing positive for coronavirus disease 2019 (COVID-19). *JAMA Cardiol.* **9**, 1036–1041 (2020).
41. Sames, E., Paterson, H. & Li, C. Hydroxychloroquine-induced agranulocytosis in a patient with long-term rheumatoid arthritis. *Eur. J. Rheumatol.* **3**, 91–92 (2016).
42. Castanheira, F. V. S. & Kubes, P. Neutrophils and NETs in modulating acute and chronic inflammation. *Blood* **133**, 2178–2185 (2019).
43. Silvestre-Roig, C. et al. Neutrophil diversity in health and disease. *Trends Immunol.* **40**, 565–583 (2019).
44. Djie, M. Z., Stone, S. R. & Le Bonniec, B. F. Intrinsic specificity of the reactive site loop of α_1-antitrypsin, α_1-antichymotrypsin, antithrombin III, and protease nexin I. *J. Biol. Chem.* **272**, 16268–16273 (1997).
45. Peiser, L., Mukhopadhyay, S. & Gordon, S. Scavenger receptors in innate immunity. *Curr. Opin. Immunol.* **14**, 123–128 (2002).
46. Lahoz-Beneytez, J. et al. Human neutrophil kinetics: modeling of stable isotope labeling data supports short blood neutrophil half-lives. *Blood* **127**, 3431–3438 (2016).
47. Bulbake, U. et al. Liposomal formulations in clinical use: an updated review. *Pharmaceutics* **9**, 12 (2017).
48. Branzk, N. et al. Neutrophils sense microbe size and selectively release neutrophil extracellular traps in response to large pathogens. *Nat. Immunol.* **15**, 1017–1025 (2014).
49. Pawlowski, C. L. et al. Platelet microparticle-inspired clot-responsive nanomedicine for targeted fibrinolysis. *Biomaterials* **128**, 94–108 (2017).
50. Stavrou, E. X. et al. Factor XII and uPAR upregulate neutrophil functions to influence wound healing. *J. Clin. Invest.* **128**, 944–959 (2018).
51. Stavrou, E. X. et al. Host and tumor factor XII drive ovarian cancer maintenance and progression. *Blood* **134**, 2384–2384 (2019).
52. Englert, H. et al. Defective NET clearance contributes to sustained FXII activation in COVID-19-associated pulmonary thrombo-inflammation. *EBioMedicine* **67**, 103382 (2021).

Publisher's note Springer Nature remains neutral with regard to jurisdictional claims in published maps and institutional affiliations.

© This is a U.S. Government work and not under copyright protection in the US; foreign copyright protection may apply 2022

Methods

Animals. Eight- to 12-week-old male and female mice in a C57BL/6J background (Jackson Laboratories) were equally used for all studies. Animal care and procedures were reviewed and approved by the Institutional Animal Care and Use Committees at Case Western Reserve University (protocol no. 2015-0109) and University of Pittsburgh (protocol no. 21110037) and performed in accordance with the guidelines of the American Association for Accreditation of Laboratory Animal Care and the National Institutes of Health.

Isolation of murine peripheral blood neutrophils. Murine peripheral blood was drawn by IVC venipuncture into sodium citrate tubes (ratio, one part anticoagulant to nine parts whole blood). Peripheral neutrophils were isolated with a magnetic bead separation system (Miltenyi Biotec) according to the manufacturer's instructions. The eluted cells were resuspended in serum-free medium without growth factors.

Human platelet, plasma and neutrophil isolation. All human blood sample studies were performed with blood from healthy individuals in accordance with a protocol approved by the Institutional Review Boards (Case 12Z05, IRB no. 09-90-195) of University Hospitals Cleveland Medical Center and the Colorado Multiple Institutional Review Board. All participants provided written informed consent. The protocol, amendments and informed consent forms were approved by the institutional review board. Eligible healthy subjects were 18 years or older; male or female; not on active medications including immunosuppressive and over the counter nonsteroidal anti-inflammatory drugs; and without diagnosis of an acute illness in the past four weeks. Whole blood was drawn by venipuncture from healthy individuals into sodium citrate tubes (ratio, one part anticoagulant to nine parts whole blood). To obtain platelet-rich plasma, whole blood was centrifuged at 150*g* for 15 min at room temperature. Platelet-rich plasma was added to a sepharose, and a HEPES-buffered saline (HBS)-containing column and droplets were collected in fractions to obtain gel filtered platelets, which were counted on a Beckman Coulter Counter. To obtain platelet-poor plasma, whole blood was centrifuged sequentially at 150*g* for 15 min, followed by 2,000*g* for 25 min at room temperature. Platelet-poor plasma supernatants were divided into 0.25 ml aliquots, transferred into clean polypropylene tubes and stored at −80 °C. Peripheral neutrophils were isolated using a magnetic bead separation system (EasySep, Stem Cell Technologies) according to the manufacturer's instructions. Eluted cells were counted using a haemocytometer and trypan blue, centrifuged at 300*g* for 10 min and resuspended in DMEM/F-12 containing 1% bovine serum albumin, 2 mM $CaCl_2$ and 2 mM $MgCl_2$ for in vitro functional assays. Platelets were activated with 20 nM thrombin, and neutrophils were activated using 1 μM fMLP, unless otherwise stated.

Ly6G–Fab generation and purification. Ly6G–Fab generation and purification was done using the Pierce Fab Preparation Kit according to the manufacturer's instructions. Briefly, the process requires equilibration of immobilized papain, preparation of Ly6G IgG samples, generation of antibody fragments and Ly6G–Fab purification steps. To assess digestion completion, we evaluated the digest and wash fractions via non-reducing sodium dodecyl sulfate–polyacrylamide gel electrophoresis. Following purification, all elutions and flow-through containing Fc and undigested IgG fragments were assessed for Fab content and purity. Protein concentration was measured by absorbance at 280 nm, using an estimated extinction coefficient of 1.4. On average, Fab yields ranged from 45–65% of the starting Ly6G antibody concentration (7.81 mg ml^{-1}).

Studies with NPs. *Confocal microscopy.* NP binding was assessed in vitro by confocal imaging using 5×10^5 human neutrophils and 1×10^7 platelets. First, platelets were stained with calcein AM (1 μg ml^{-1} final concentration) prior to incubation with neutrophils or NPs. Next, neutrophils, platelets and 3×10^9 ml^{-1} NPs (U-NP, NEBP-NP, PBP-NP or PNT-NP) were mixed before being added to slides and were incubated for 2 hours at 37 °C in the presence of 1 μM fMLP and 20 nM thrombin. On completion of incubation, slides were gently washed with PBS, fixed with 4% paraformaldehyde for 5 min, washed again with PBS, mounted with VectaShield DAPI mounting solution and cover-slipped. Slides were imaged using a Leica HyVolution SP8 confocal microscope, and fluorescent intensity was quantified using ImageJ 2.0.0 software (National Institutes of Health).

Flow cytometry. Flow cytometry experiments used 1×10^6 ml^{-1} neutrophils and 3×10^9 ml^{-1} NPs per tested condition. Human neutrophils were either left untreated or were stimulated with 1 μM fMLP and incubated with U-NPs or PNT-NPs for 1 hour at 37 °C. Following a washing step with PBS, cells were fixed with 1% paraformaldehyde for 15 min at room temperature. After additional washing steps, samples were centrifuged at 600*g* for 10 min, resuspended in 400 μl of PBS and placed on ice until analysis. Neutrophils were gated based on forward and side scatter characteristics. At least 10,000 cells gated from forward and side scatter characteristics were acquired for analysis, and RhB fluorescent intensity (detection channel YG610A) was measured for each group using a LSR II flow cytometer (BD Biosciences). Images were acquired for analysis using BD FACSDiva software (BD Biosciences). Data analysis was performed with FlowJo 10.4.2 software.

Similarly, human platelets (1×10^7 ml^{-1}) were either left untreated or were activated with 20 nM thrombin and incubated with PNT-NPs. Cells were first sorted by scatter and CD42b positivity (B525A; 1:100 dilution). Then, activated platelets were gated by CD62P+ (1:100 dilution; detection channel R600A), followed by gating for RhB fluorescence. For studies with NEBP-NPs, purified human neutrophils were treated with or without 10 ng ml^{-1} TNF-α, 5 μg ml^{-1} LPS or 1 μM fMLP and coincubated with RhB-labelled NEBP-NPs for 1 hour at 37 °C. Following a washing step with PBS, cells were fixed with 1% paraformaldehyde for 8 min at room temperature. After additional washing steps, samples were centrifuged at 600*g* for 10 min, resuspended in 400 μl of FACS buffer and placed on ice until analysis. Cells were gated based on forward and side scatter characteristics and initially sorted by CD66b (AF700; 1:100 dilution) positivity, followed by doublet discrimination and gating for NE (Cy5; 1:100 dilution). The percentage of CD66b and NE double positive single cells in complex with NEBP-NPs was determined by measuring RhB fluorescent intensity (YG610A).

Additional methods are provided in the Supplementary Information.

Statistical analysis. All data are presented as mean ± standard error of the mean (s.e.m.) unless otherwise indicated and with the indicated sample size. Difference between two groups was determined by unpaired two-tailed Student's *t*-test. One-way ANOVA analysis with Bonferroni post-hoc analysis was used to compare three or more related groups. To determine if soluble P-selectin interferes with PBP-NP binding to surface-exposed P-selectin, we employed ordinary one-way ANOVA with Dunnett's multiple comparisons test. NP half-life and PNT-NP binding to neutrophils and platelets (flow cytometry) were calculated with ordinary two-way ANOVA. Prism 9.0.0 (GraphPad), FlowJo 10.4.2, ImageJ 2.0.0, CellSens v.1.18, MO.Affinity Analysis v.2.3 and SoftMax Pro VS.4.5 software were used for analysis. A P value of <0.05 was considered significant.

Reporting summary. Further information on research design is available in the Nature Research Reporting Summary linked to this article.

Data availability

Modelling of docking complex with highlighted reactive centre loop and NEBP was performed using native AAT (Protein Data Bank code 1QLP)[20,21]. The authors declare that data supporting the findings of this study are available in their entirety within the article and its Supplementary Information. Relevant data can be provided by the corresponding authors upon reasonable request.

Acknowledgements

We thank the Hematopoietic Biorepository Core of Case Western Reserve University for human blood sample provision; M. Sramkoski at the Case Western Reserve University Cancer Center Flow Cytometry core facility; S. Bandyopadhyay at the Cleveland Clinic for assistance with BiaCore studies; and G. Deshpande and the Cleveland Clinic Lerner Research Institute Imaging Core for expert histologic analysis. This work was supported by the National Institutes of Health R01 HL137695 (E.X.S.); R01 HL129179, R01 HL137695, R01 HL141080, R01 HL121212 (A.S.G.); R33HL141794, R01HL120728, R01HL151984 (K.B.N.); R35 GM119526, R01 HL141080 (M.D.N.); R01 HL098217 (M.T.N.); EY022938, R24 EY024864 (T.S.K.); F32 HL149207 (J.A.); the Clinical and Translational Science Collaborative of Cleveland [UL1TR002548 from the National Center for Advancing Translational Sciences component of the National Institutes of Health and National Institutes of Health roadmap for Medical Research (E.X.S., A.S.G.)]; Merit Review Awards (BX003851 (E.X.S.) and BX003604 (T.S.K.) from the Department of Veterans Affairs); a Case Coulter Translational Research Partnership Award (RES514649 (E.X.S., A.S.G.)); a University of Pittsburgh Physician-Scientist Award from the Burroughs Wellcome Fund (E.A.A., J.A.); a T-32 PostDoctoral Training award [NIH T32HL098036 (E.A.A.)]; an American Heart Association Scientist Development Award (E.X.S.); and the Oscar D. Ratnoff Endowed Professorship (E.X.S.). We acknowledge an unrestricted grant to the Department of Ophthalmology from Research to Prevent Blindness (New York, NY; T.S.K.). S.d.M. gratefully acknowledges the Toegepaste en Technische Wetenschappen (TTW) section of the Netherlands Organization for Scientific Research (NWO, 2019/TTW/00704802). The contents are solely the responsibility of the authors and do not necessarily represent the official views of the National Institutes of Health, the US Department of Veterans Affairs or the United States Government.

Author contributions

M.A.C., D.B., E.A.A., M.T.N., T.S.K., K.B.N., C.M., S.d.M., M.D.N., A.S.G. and E.X.S. conceptualized and planned the experiments. M.A.C., D.B., E.A.A., J.A., S.R., N.A.M., N.D.v.K., K.L.B., S.H., K. Hageman, K.M., M.S., H.L., A.B., E.M.L., K. Hart, A.G., M.d.l.F. and E.X.S. performed the experiments. M.A.C., S.d.M., A.S.G. and E.X.S. prepared the figures. M.A.C. and E.X.S. wrote the manuscript, and all authors reviewed and edited the manuscript before submission.

Competing interests

A.S.G. is a coinventor on issued patent US 9107845 (Synthetic Platelets) that is licensed from Case Western Reserve University to Haima Therapeutics. A.S.G. is a cofounder and equity stakeholder of Haima Therapeutics. The patent is on the design of a heteromultivalent NP system that can mimic the haemostatic functions of a platelet.

A.S.G. is also a coinventor on issued patent US 9107963 (Heteromultivalent Nanoparticle Compositions). The patent is on the design of heteromultivalently decorated NPs for clot targeting. Although the specific NP systems described in these two patents have no direct relevance to any specific aspect of the manuscript, the context of 'heteromultivalent NP design' is a central aspect of the NT-NP and PNT-NP systems described in the manuscript. M.D.N. serves on the scientific advisory board of Haima Therapeutics and holds equity stake. E.X.S. is coinventor of intellectual property that has been licensed by Case Western Reserve University to XaTek and receives royalties. The patent PCT/US2017/013797 is on dielectric spectroscopy for whole blood assessment of haemostasis. This patent bears no relevance to any of the work presented in the manuscript. C.M. has been a speaker for Shire-Takeda. C.M. and S.d.M. are cofounders of TargED BV, a biotech spinout company of University Medical Center Utrecht (based upon the WO2019185723 A1 patent). C.M. and S.d.M. participate in revenue sharing as inventors through the commercialization arm of the University Medical Center Utrecht. The remaining authors declare no competing interests.

Additional information

Supplementary information The online version contains supplementary material available at https://doi.org/10.1038/s41565-022-01161-w.

Correspondence and requests for materials should be addressed to Anirban Sen Gupta or Evi X. Stavrou.

Peer review information *Nature Nanotechnology* thanks Benoit Ho-Tin-Noé, Zoltan Jakus and Guillermo Ruiz-Esparza for their contribution to the peer review of this work.

Reprints and permissions information is available at www.nature.com/reprints.

nature research

Corresponding author(s): Evi X. Stavrou
Anirban Sen Gupta

Last updated by author(s): May 10, 2022

Reporting Summary

Nature Research wishes to improve the reproducibility of the work that we publish. This form provides structure for consistency and transparency in reporting. For further information on Nature Research policies, see our Editorial Policies and the Editorial Policy Checklist.

Statistics

For all statistical analyses, confirm that the following items are present in the figure legend, table legend, main text, or Methods section.

n/a	Confirmed
☐	☒ The exact sample size (*n*) for each experimental group/condition, given as a discrete number and unit of measurement
☐	☒ A statement on whether measurements were taken from distinct samples or whether the same sample was measured repeatedly
☐	☒ The statistical test(s) used AND whether they are one- or two-sided *Only common tests should be described solely by name; describe more complex techniques in the Methods section.*
☒	☐ A description of all covariates tested
☒	☐ A description of any assumptions or corrections, such as tests of normality and adjustment for multiple comparisons
☐	☒ A full description of the statistical parameters including central tendency (e.g. means) or other basic estimates (e.g. regression coefficient) AND variation (e.g. standard deviation) or associated estimates of uncertainty (e.g. confidence intervals)
☐	☒ For null hypothesis testing, the test statistic (e.g. *F*, *t*, *r*) with confidence intervals, effect sizes, degrees of freedom and *P* value noted *Give P values as exact values whenever suitable.*
☒	☐ For Bayesian analysis, information on the choice of priors and Markov chain Monte Carlo settings
☒	☐ For hierarchical and complex designs, identification of the appropriate level for tests and full reporting of outcomes
☒	☐ Estimates of effect sizes (e.g. Cohen's *d*, Pearson's *r*), indicating how they were calculated

Our web collection on statistics for biologists contains articles on many of the points above.

Software and code

Policy information about availability of computer code

Data collection	Flow cytometry data were obtained using BD FACSDiva Software 80.1. Substrate conversion and clot-lysis data were obtained on a SpectraMax M2 from Molecular Devices in combination with the SoftMax Prof Software V5.4.5. Microfluidic studies were conducted on Olympus microscopes (FV10i, IX81 Yokagawa CSU) with 60X (NA 1.35) oil immersion objectives, and CMOS cameras (Hamamatsu, Orca Flash4.0) using CellSens software v.1.18.
Data analysis	Most data were analyzed with Graph Pad Prism 9.0.0 software. Immunofluorescence images were quantitated using ImageJ NIH software. Co-localization between neutrophils and adherent nanoparticles was determined using the Manders' overlap coefficients. Before calculation of the Manders' overlaps, we applied automatic and user bias-free Costes thresholding implemented in ImageJ 2.0.0 software (plug-in JACoP). Flow cytometry data were analyzed by FlowJo 10.4.2 software. Microscale thermophoresis results were analyzed with MO.Affinity Analysis v.2.3 software.

For manuscripts utilizing custom algorithms or software that are central to the research but not yet described in published literature, software must be made available to editors and reviewers. We strongly encourage code deposition in a community repository (e.g. GitHub). See the Nature Research guidelines for submitting code & software for further information.

Data

Policy information about availability of data

All manuscripts must include a data availability statement. This statement should provide the following information, where applicable:

- Accession codes, unique identifiers, or web links for publicly available datasets
- A list of figures that have associated raw data
- A description of any restrictions on data availability

Modeling of docking complex with highlighted RCL and NEBP was performed using native AAT [Protein Data Bank (PDB) code 1QLP [Elliott, P. R., Lomas, D. A.,

Carrell, R. W. et al. Inhibitory conformation of the reactive loop of alpha 1-antitrypsin. Nat Struct Biol 3, 676-681, (1996)]; [Elliott, P. R., Pei, X. Y., Dafforn, T. R. et al. Topography of a 2.0 A structure of alpha1-antitrypsin reveals targets for rational drug design to prevent conformational disease. Protein Sci 9, 1274-1281, (2000)]. The authors declare that data supporting the findings of this study are available in their entirety within the article and its Supplementary Information. Relevant data can be provided by the corresponding authors (E.X.S., A.S.G.) upon reasonable request.

Field-specific reporting

Please select the one below that is the best fit for your research. If you are not sure, read the appropriate sections before making your selection.

☒ Life sciences ☐ Behavioural & social sciences ☐ Ecological, evolutionary & environmental sciences

For a reference copy of the document with all sections, see nature.com/documents/nr-reporting-summary-flat.pdf

Life sciences study design

All studies must disclose on these points even when the disclosure is negative.

Sample size	No statistical methods were used to predetermine the sample size. Sample sizes for experiments were estimated based on previous experiences and reports with similar setups that showed significance, for example, PMCID: PMC5920765 for microfluidic studies; PMCID: PMC6866660 for retinal studies; PMID 29391442, 31294514 from our group and (PMID 20959603) for IVC ligation experiments; PMID: 31220416 and PMID: 28314136 for in vivo nanoparticle administration; PMID: 29376892 for surface plasmon resonance and immunofluorescent studies with neutrophils. Sample size for individual data sets are described in figure legends.
Data exclusions	Animals who died prior to 24 hour sacrifice time point and animals who formed no clots were excluded from analysis. For all other studies outlined in this manuscript, no data were excluded from analyses.
Replication	All experiments were conducted at least three times, the number of experimental replicates for individual assays is specified. All attempts at replication were successful. IVC ligation experiments were repeated on 7 separate days by the same trained animal surgeon to ensure replication.
Randomization	Particles were randomly assigned to different surface functionalization. Cells were randomly assigned to experimental groups with different treatments. Animals were also randomly assigned to various treatments.
Blinding	IVC ligation experiments were conducted by a single investigator who was blinded to prior results. Particles were labeled without identifying features and were identical in appearance. Equal numbers of animals were conducted for each set of particles on the same days to limit day to day or batch to batch variability.

Reporting for specific materials, systems and methods

We require information from authors about some types of materials, experimental systems and methods used in many studies. Here, indicate whether each material, system or method listed is relevant to your study. If you are not sure if a list item applies to your research, read the appropriate section before selecting a response.

Materials & experimental systems

n/a	Involved in the study
☐	☒ Antibodies
☐	☒ Eukaryotic cell lines
☒	☐ Palaeontology and archaeology
☐	☒ Animals and other organisms
☐	☒ Human research participants
☒	☐ Clinical data
☒	☐ Dual use research of concern

Methods

n/a	Involved in the study
☒	☐ ChIP-seq
☐	☒ Flow cytometry
☒	☐ MRI-based neuroimaging

Antibodies

Antibodies used	Anti-mouse Ly6G antibody (clone 1A8; Catalogue #BE0075-1; Lot #626716O1) was purchased from BioXCell. Primary antibodies to neutrophil elastase (rabbit anti-human; Abcam; Catalog #ab183342; Lot #GR3215601-2); Polyclonal rabbit Neutrophil Elastase antibody, Cy5-conjugated (Bioss Antibodies, Catalog # bs-6982R-Cy, Lot #: AF02149519); FITC Ly6G/Ly6C (rat anti-mouse, clone RB6-8C5; BioLegend; Catalogue #108417; Lot #B229994), CD62P (AF647-conjugated mouse anti-human, clone AK4; Biolegend; Catalogue #304918; Lot #B260906), CD42b (FITC-conjugated mouse anti-human, clone HIP1; BD biosciences; Catalogue #561855; Lot #9079862), CD16 (APC-conjugated mouse anti-human, clone3G8; Biolegend; Catalogue #302011; Lot #B300869), MMP9 (FITC-conjugated mouse anti-human, clone 56129; R&D Systems; Catalogue #IC9111F; Lot #LKB0819041), CD66b (AF700-conjugated mouse anti-human, clone G10F5; Biolegend; Catalogue #305113; Lot #b267050), citrullinated histone H3 (rabbit anti-human, clone ab5103; Abcam; Catalogue #ab5103; Lot #GR3362159-1), were used for immunostaining and flow cytometry experiments. Secondary antibody to neutrophil elastase (488-conjugated AlexaFluor donkey anti-rabbit; Catalogue #A-21206; Lot #1796375) was from ThermoFisher. Anti-rabbit PE antibody (Catalogue #F0110; Lot #AEANO318122) was from R&D Systems.

Validation	All antibodies were commercially available and were validated by manufacturers, in previous publications, and in this study, and used for the specific indications suggested by manufacturers. - Anti-mouse Ly6G antibody (BioXCell) is validated by the vendor and is cited by 19 peer reviewed papers (https://bxcell.com/product/invivoplus-anti-m-ly-6g-2/) - Rabbit anti-human Ab to NE (Abcam) is validated by the vendor (https://www.abcam.com/neutrophil-elastase-antibody-sp203-ab183342.html). Our lab has also validated this Ab in spleen and liver for specificity (data not presented in this manuscript but available at request) - FITC Ly6G/Ly6C (rat anti-mouse, BioLegend) is quality controlled and validated by the vendor and has been cited in 19 peer reviewed publications (https://www.biolegend.com/en-us/products/alexa-fluor-488-anti-mouse-ly-6g-ly-6c-gr-1-antibody-2711) - CD62P (AF647-conjugated mouse anti-human, Biolegend) is quality controlled by the vendor and has been cited in 5 peer reviewed publications (https://www.biolegend.com/en-us/products/alexa-fluor-647-anti-human-cd62p-p-selectin-antibody-3348). - Polyclonal rabbit Neutrophil Elastase antibody, Cy5-conjugated (Bioss Antibodies) is validated by the vendor and has been cited in 14 peer reviewed publications (https://www.biossusa.com/products/bs-6982r-cy5). - CD42b (FITC-conjugated mouse anti-human, BD biosciences) is validated by the vendor and has been cited specifically for flow cytometry applications in 4 peer reviewed publications (https://www.bdbiosciences.com/us/reagents/research/antibodies-buffers/immunology-reagents/anti-human-antibodies/cell-surface-antigens/fitc-mouse-anti-human-cd42b-hip1/p/561855) - CD16 (APC-conjugated mouse anti-human, Biolegend) is validated by the vendor and has been cited by 24 peer reviewed publications https://www.biolegend.com/en-us/products/apc-anti-human-cd16-antibody-565) - MMP9 (FITC-conjugated mouse anti-human, R&D Systems) is validated by the vendor and has been cited by 6 peer reviewed publications (https://www.rndsystems.com/products/human-mmp-9-fluorescein-conjugated-antibody-56129_ic9111f#product-citations) - CD66b (AF700-conjugated mouse anti-human, Biolegend) is validated by the vendor and has been cited by 6 peer reviewed publications (https://www.biolegend.com/en-us/products/alexa-fluor-700-anti-human-cd66b-antibody-12098) - Citrullinated histone H3 (rabbit anti-human, Abcam) is validated by the vendor and has been cited by 250 peer reviewed publications (https://www.abcam.com/histone-h3-citrulline-r2--r8--r17-antibody-ab5103.html) - Anti-rabbit PE antibody, R&D Systems is quality controlled by the vendor and is cited by 2 publications (https://www.rndsystems.com/products/rabbit-igg-pe-conjugated-antibody_f0110#product-citations) - 488-conjugated AlexaFluor donkey anti-rabbit (ThermoFisher) is quality controlled by the vendor and is cited by 400 publications (https://www.thermofisher.com/antibody/product/Donkey-anti-Rabbit-IgG-H-L-Highly-Cross-Adsorbed-Secondary-Antibody-Polyclonal/A-21206).

Eukaryotic cell lines

Policy information about cell lines

Cell line source(s)	HEK-293 cell line was sourced from ATCC.
Authentication	The cell lines were certified by the manufacturers (surface markers, morphology).
Mycoplasma contamination	None detected.
Commonly misidentified lines (See ICLAC register)	No commonly misidentified cell lines were used.

Animals and other organisms

Policy information about studies involving animals; ARRIVE guidelines recommended for reporting animal research

Laboratory animals	Eight- to 12-week-old male and female mice in a C57BL/6J background (Jackson Laboratories) were equally used for all studies.
Wild animals	The study did not involve wild animals.
Field-collected samples	The study did not involve samples collected from the field.
Ethics oversight	Eight- to 12-week-old male and female mice in a C57BL/6J background (Jackson Laboratories) were equally used for all studies. Mice were housed in University animal facilities under specific pathogen-free conditions and at a 12-hour light/12-hour dark cycle. Temperatures of 68-75°F with 40-60% humidity were maintained. Animal care and procedures were reviewed and approved by the Institutional Animal Care and Use Committees at Case Western Reserve University (protocol #2015-0109) and University of Pittsburgh (protocol #21110037) and performed in accordance with the guidelines of the American Association for Accreditation of Laboratory Animal Care and the National Institutes of Health.

Note that full information on the approval of the study protocol must also be provided in the manuscript.

Human research participants

Policy information about studies involving human research participants

Population characteristics	Eligible healthy subjects were 18 years or older, male and female; were not on active medications including immunosuppressive and over the counter nonsteroidal anti-inflammatory drugs (NSAIDs); and were without diagnosis of an acute illness in the past 4 weeks. There was no age, gender or other selection bias.

Recruitment	Participants were accrued through flier advertising across the CWRU Medical Campus and University of Colorado Denver
Ethics oversight	All human blood sample studies were performed with blood from healthy individuals in accordance with a protocol approved by the Institutional Review Board (Case 12Z05, IRB # 09-90-195) of University Hospitals Cleveland Medical Center and the Colorado Multiple Institutional Review Board (COMIRB). All participants provided written informed consent. The protocol, amendments, and informed consent forms were approved by the institutional review board.

Note that full information on the approval of the study protocol must also be provided in the manuscript.

Flow Cytometry

Plots

Confirm that:

☒ The axis labels state the marker and fluorochrome used (e.g. CD4-FITC).

☒ The axis scales are clearly visible. Include numbers along axes only for bottom left plot of group (a 'group' is an analysis of identical markers).

☒ All plots are contour plots with outliers or pseudocolor plots.

☒ A numerical value for number of cells or percentage (with statistics) is provided.

Methodology

Sample preparation	For flow cytometry studies with hydroxychloroquine-loaded nanoparticles (HCQ_PNT-NP, HCQ_NEBP-NP, HCQ_PBP-NP), neutrophils from human healthy individuals were purified from peripheral whole blood using negative immunomagnetic separation. Purified neutrophils were resuspended in DMEM-F12 containing 2mM MgCl2 and 2mM CaCl2. Cells were stimulated with 1 µM fMLP for two hours at 37°C and 5% CO2, in the absence or presence of 350 ng/ml free HCQ or HCQ-loaded PNT-NP. Neutrophils were spun down at 2000 x g for 5 min at 4°C, resuspended in HEPES containing 10% FBS for 30 minutes on ice. ========== For flow cytometry studies with empty NPs(U-NP), unloaded NPs [2 groups: untargeted (U-NP) and targeted/decorated (PNT-NP, PBP-NP, NEBP-NP), respectively], human neutrophils were similarly isolated and processed, as mentioned above. To obtain platelet rich plasma (PRP), whole blood was centrifuged at 12,000g for 25 min at room temperature. PRP was added to a sepharose and HBS-containing column and droplets were collected in fractions to obtain gel filtered platelets which were counted on a Beckman Coulter Counter. To obtain platelet poor plasma (PPP), whole blood was centrifuged sequentially at 3,000g for 30 min, followed by 11,000g for 10 min at room temperature. PPP supernatants were divided into 0.25 ml aliquots, transferred into clean polypropylene tubes, and stored at -80°C. Human neutrophils were stimulated with 1 µM fMLP and incubated with NPs for 1 hour at 37°C. Following a washing step with PBS, cells were fixed with 1% PFA for 15 min at room temperature. After additional washing steps, samples were centrifuged at 600 x g for 10 min, resuspended in 400 µl of PBS and placed on ice until analysis.
Instrument	LSR II flow cytometer, BD Biosciences
Software	Data acquisition was performed with BD FACSDIVA Software; Flow cytometry analysis was performed with FlowJo 10.4.2 software. For statistical comparison, data were analyzed with Prism 9.0 software.
Cell population abundance	At least 10,000 cells gated from forward and side-scatter characteristics were acquired for all FACS analysis.
Gating strategy	All cells were gated based on forward and side-scatter characteristics to limit debris including dead cells and particles. Gating of "Positive" and "negative" biomarker staining are specified in figures and supplementary figures. Specifically: - Experiments to determine binding of PNT-NP to activated neutrophils and platelets: Neutrophils were gated based on forward and side scatter characteristics. At least 10,000 events within the neutrophil gate were collected for analysis. Similarly, human platelets (1 x 10^7) were activated with 20 nM thrombin and incubated with U-NP or PNT-NP. Cells were first sorted by scatter and CD42b positivity (B525A). Then, activated platelets were gated by CD62P + (R600A), followed by gating for rhodamine B fluorescence. ========== - Experiments to measure binding of NEBP-NP to activated neutrophils: Cells were gated based on forward and side scatter characteristics and initially sorted by CD66b (AF700) positivity, followed by doublet discrimination and gating for neutrophil elastase [(NE), Cy5]. The percentage of CD66b and NE double positive single cells in complex with NEBP-NP was determined by measuring rhodamine B (RhB) fluorescent intensity (YG610A). ========== - For determination of NETs, neutrophils were defined as CD16, CD66b, and MMP9 triple positive cells. Neutrophil H3Cit expression was quantified and expressed as % change in median fluorescent intensity compared to unstimulated neutrophils.

☒ Tick this box to confirm that a figure exemplifying the gating strategy is provided in the Supplementary Information.